Black hole formation from the gravitational collapse of a nonspherical network of structures

Ismael Delgado Gaspar,[1,*] Juan Carlos Hidalgo,[2,†] Roberto A. Sussman,[1,‡] and Israel Quiros[3,§]

[1]*Instituto de Ciencias Nucleares, Universidad Nacional Autónoma de México (ICN-UNAM),*
A.P. 70-543, 04510 México D.F., Mexico
[2]*Instituto de Ciencias Físicas, Universidad Nacional Autónoma de México,*
62210 Cuernavaca, Morelos, Mexico
[3]*Departamento Ingeniería Civil, División de Ingeniería, Universidad de Guanajuato,*
36000 Guanajuato, Mexico

We examine the gravitational collapse and black hole formation of multiple nonspherical configurations constructed from Szekeres dust models with positive spatial curvature that smoothly match to a Schwarzschild exterior. These configurations are made of an almost spherical central core region surrounded by a network of "pancake-like" overdensities and voids with spatial positions prescribed through standard initial conditions. We show that a full collapse into a focusing singularity, without shell crossings appearing before the formation of an apparent horizon, is not possible unless the full configuration becomes exactly or almost spherical. Seeking for black hole formation, we demand that shell crossings are covered by the apparent horizon. This requires very special fine-tuned initial conditions that impose very strong and unrealistic constraints on the total black hole mass and full collapse time. As a consequence, nonspherical nonrotating dust sources cannot furnish even minimally realistic toy models of black hole formation at astrophysical scales: demanding realistic collapse time scales yields huge unrealistic black hole masses, while simulations of typical astrophysical black hole masses collapse in unrealistically small times. We note, however, that the resulting time-mass constraint is compatible with early Universe models of primordial black hole formation, suitable in early dust-like environments. Finally, we argue that the shell crossings appearing when nonspherical dust structures collapse are an indicator that such structures do not form galactic mass black holes but virialize into stable stationary objects.

I. INTRODUCTION

The gravitational collapse and black hole (BH) formation (including singularity censorship issues) of spherically symmetric dust models has been extensively examined [1]. These models are described by the Lemaître-Tolman-Bondi (LTB) solutions and typically consider a dust overdensity (a local spatial density maximum) around the symmetry centre.

However, the proper study of BH formation from the collapse of nonspherical dust configurations remains an open problem (see [2,3]). In particular, the quasispherical Szekeres solutions of class I [4–6] allow for modeling nontrivial nonspherical configurations, involving a spheroidal overdensity or density void surrounded by elaborated networks of "pancake-like structures." Here, by pancake-like structures we mean elongated regions that contain local

spatial density maxima (overdensities) or minima (voids), which can be localized in terms of radial and angular coordinates of suitable spherical comoving coordinates. As shown in [7–10], these Szekeres models allow for prescribing the spatial location of all these extremes from specified initial conditions.

Since quasispherical Szekeres models are the least idealized exact solution applicable to cosmology, there is a large body of literature employing them as toy models for structure formation and for fitting cosmological observations [7–13]. However, the proper study of BH formation from quasispherical Szekeres models, and indeed from any nonspherical progenitors, remains largely unexplored. In this context, Ref. [14] discusses the conditions for BH formation from the collapse of Szekeres configurations, while the definition of their apparent horizon is discussed in [15]. These references stand as valuable precedents, but still leave important issues to be examined. In particular, in astrophysical systems it is plausible to match the Szekeres central solution to a Schwarzschild exterior. Therefore from the outside the process is seen as the usual spherical

---
*[*]ismael.delgado@correo.nucleares.unam.mx
[†]hidalgo@fis.unam.mx
[‡]sussman@nucleares.unam.mx
[§]iquiros@fisica.ugto.mx

collapse. However, we are interested in the nonspherical interior and the evolution of multiple (pancake-like and spherical) structures. The aim of the present article is to explore the collapse of networks of nonspherical structures modeled by Szekeres solutions into a single "big crunch" singularity (final focusing singularity).

We find advantageous to address the problem employing quasilocal scalar variables adapted to Szekeres models (a formalism developed in [10,16–18]). Such formalism is idoneous to describe the complex radial and angular dependence of the density associated with these networks of structures, and their specification through initial conditions. Besides these advantages, the q-scalars and their fluctuations are exact generalizations of cosmological dust perturbations in the synchronous (and comoving) gauge of cosmological perturbation theory [18,19].

In previous work [17] we were concerned with cosmic structure modeling, looking at localized collapsing regions within models whose cosmic background (a Λ cold dark matter background) is expanding. Consequently we considered only two types of "collapse morphologies" (defined by the three eigenvalues of the expansion tensor): the "spherical" collapse (all negative eigenvalues) and the "pancake" collapse (two positive and one negative eigenvalues). Under this approach we simply assumed that locally collapsing regions (spherical or pancake) would virialize into stationary stable structures and thus ignored their terminal evolution into singularities (big crunch or shell crossings).

In this paper we are interested in astrophysical BH formation from multiple overdensities. We model local collapse (with $\Lambda = 0$) of configurations with positive spatial curvature consisting of a central LTB inhomogeneity, surrounding Szekeres pancake solutions and embedded in an exterior Schwarzschild spacetime (see Fig. 2 below). We simulate the gravitational collapse through examples evolving the pure growing mode of the Szekeres structures and find that a full big crunch collapse without shell crossings appearing before the formation of an apparent horizon is not possible unless the full configuration becomes exactly or almost spherical. This is a consequence of the fact that conditions for avoiding shell crossings are much more stringent in Szekeres models than in LTB models. Our results indicate that the setup may represent a suitable model for large-scale structure formation in which the dust structures eventually enter a stage of virialization beyond the Szekeres description [20].

Looking for the possibility of BH formation of fully nonspherical configurations with this proviso, we fine-tune the initial conditions, so that shell crossings become covered by the apparent horizon and lie very close to (what would be) the locus of the big crunch. For such examples, we compute the final collapse time and total BH mass. Our results show either a very short time of collapse or a very large mass of the BH developed over astrophysical timescales. Instead, our results show compatibility with the

theory of primordial black holes (PBH) formation, which involves a rapid collapse of very small masses [14,21,22].

The plan of the paper is as follows. In Sec. II we introduce a description of the Szekeres models in terms of q-scalars and spherical coordinates and comment on sufficient conditions for the existence of multiple spatial extrema of the Szekeres scalars. General features of the quasispherical Szekeres models are reviewed in Sec. III including the collapse morphologies, a criterium for the identification of apparent horizons, and the occurrence of shell crossings and concavity inversions points (the evolving of local density maxima into local minima and vice versa). In this section we argue that shell crossings are indicative of the start of virialization, therefore we can model the structure formation process. To illustrate our setup, in Sec. IV we show two representative examples of structure formation with Szekeres models, namely, a galaxy supercluster and a BH. Our results are summarized and discussed in Sec. V. Finally, we have included four appendices that complement the main text. Appendixes A and B provide the evolution equations of the q-scalars and metric functions in Szekeres models and their exact solution for $\Lambda = 0$, respectively. These solutions are rewritten in a dimensionless form in Appendix C, and in Appendix D we list the general conditions to avoid shell crossings.

II. SZEKERES MODELS IN SPHERICAL COORDINATES

The quasispherical Szekeres models of class I.[1] in terms of "stereographic" spherical coordinates are described by the metric [5],

$$ds^2 - dt^2 + a^2 h_{ij} dx^i dx^j, \quad i, j = r, \theta, \phi, \quad (1)$$

where $a = a(t, r)$ and

$$h_{rr} = \frac{(\Gamma - \mathbf{W})^2}{1 - \mathcal{K}_{qi} r^2} + (\mathcal{P} + \mathbf{W}_{,\theta})^2 + U^2 \mathbf{W}_{,\phi}^2, \quad (2)$$

$$h_{r\theta} = -r(\mathcal{P} + \mathbf{W}_{,\theta}), \quad (3)$$

$$h_{r\phi} = -rU\mathbf{W}_{,\phi}, \qquad h_{\theta\theta} = r^2, \qquad h_{\phi\phi} = r^2\sin^2\theta, \quad (4)$$

with

$$\Gamma = 1 + \frac{ra'}{a}, \qquad U = 1 - \cos\theta, \quad (5)$$

---

[1]All further mention of "Szekeres models" will refer only to quasispherical models of class I (see [5] for a broad discussion on their classification). We are not considering models whose constant time slices have spherical or wormhole topology [5] (the appropriate form of the metric (1) for those cases is given in Appendix D of [16]).

$$\mathcal{P} = X\cos\phi + Y\sin\phi, \qquad \mathbf{W} = -\mathcal{P}\sin\theta - Z\cos\theta, \quad (6)$$

and four free parameters $X, Y, Z, \mathcal{K}_{qi}$ which depend only on r [see interpretation of $\mathcal{K}_{qi}$ in (10)]. The function $\mathbf{W}$ has the mathematical structure of a dipole and governs the deviation from spherical and axial symmetries [10]. Therefore, different particular cases follow by specializing this function: $X = Y = Z = \mathbf{W} = 0$ corresponds to the spherically symmetric LTB models, while $X = Y = 0$, $Z \neq 0$ so that $\mathbf{W} = \mathbf{W}(r, \theta) = -Z\cos\theta$ corresponds to axial symmetry.

A. Quasilocal scalars and their fluctuations

To look at the dynamics of the models we introduce the quasilocal variables (q-scalars) A_q for each covariant scalar $A = \rho, H = \Theta/3, \mathcal{K} = {}^{(3)}\mathcal{R}/6$, (density, Hubble expansion and spatial curvature)

$$A_q = \frac{\int_{\mathcal{D}} AF d\mathcal{V}_p}{\int_{\mathcal{D}} F d\mathcal{V}_p}, \quad \text{with}$$

$$d\mathcal{V}_p = \sqrt{\det(g_{ij})}d^3x = \frac{a^3 r^2 (\Gamma - \mathbf{W})\sin\theta}{\sqrt{1 - \mathcal{K}_{qi}r^2}}drd\theta d\phi, \quad (7)$$

while their exact fluctuations ($\mathbf{D}^{(A)}$) are given by [16]

$$\mathbf{D}^{(A)} = A - A_q = \frac{rA_q'}{3(\Gamma - \mathbf{W})}, \quad (8)$$

$$\Delta^{(\rho)} = \frac{\mathbf{D}^{(\rho)}}{\rho_q} = \frac{\rho - \rho_q}{\rho_q}, \quad (9)$$

which lead to the following scaling laws[2]:

$$\rho_q = \frac{\rho_{qi}}{a^3}, \qquad \mathcal{K}_q = \frac{\mathcal{K}_{qi}}{a^2}, \qquad H_q = \frac{\dot{a}}{a}, \quad (10)$$

$$1 + \Delta^{(\rho)} = \frac{1 + \Delta_i^{(\rho)}}{\mathcal{G}}, \qquad \frac{2}{3} + \Delta^{(\mathcal{K})} = \frac{\frac{2}{3} + \Delta_i^{(\mathcal{K})}}{\mathcal{G}}, \quad (11)$$

$$\mathcal{G} = \frac{\Gamma - \mathbf{W}}{1 - \mathbf{W}}. \quad (12)$$

Here we have assumed the radial coordinate gauge $a_i = \Gamma_i = \mathcal{G}_i = 1$ with $_i$ denoting evaluation at an arbitrary $t = t_i$.

---

[2]The integral in (7) is evaluated in an arbitrary time slice (constant t) in a spherical comoving domain $\mathcal{D}$ bounded by an arbitrary fixed $r > 0$. The lower bound is the locus $r = 0$, analogous to the symmetry centre of spherical models [9]. While Szekeres models are not spherically symmetric, the surfaces of constant r are nonconcentric 2-spheres [5]. Notice that $A_q = A_q(t, r)$ even if the scalars A depend on the four coordinates (t, r, θ, ϕ) [16].

The q-scalars and their fluctuations are covariant objects [16] reduced in the linear limit to standard variables of cosmological dust perturbations in the synchronous gauge [18,19].

B. Spatial location of the extrema of the Szekeres scalars

The spatial location of the scalars extrema follows from the condition $A' = A_{,\theta} = A_{,\phi} = 0$, whose solutions are

$$r = r_{e\pm}, \quad \theta_\pm(r_{e\pm}), \quad \phi_\pm(r_{e\pm}), \quad \text{at } t = \text{const.} \quad (13)$$

where the angular extrema are given by

$$\phi_- = \arctan\left(\frac{Y}{X}\right), \qquad \phi_+ = \pi + \phi_-, \quad (14)$$

$$\theta_- = \arccos\left(\frac{Z}{\sqrt{X^2 + Y^2 + Z^2}}\right), \qquad \theta_+ = \pi - \theta_-. \quad (15)$$

The extrema define an angular direction for every fixed r, and the two "curves of angular extrema" $\mathcal{B}_\pm(r) = [r, \theta_\pm(r), \phi_\pm(r)]$, parametrized by r in all time slices.

A sufficient condition for the existence of an arbitrary number of radial extrema of the Szekeres scalars is achieved by assuming a sequence of "local homogeneity spheres," defined by the vanishing at all times of the shear and electric Weyl tensors along a comoving 2-sphere of generic radius r_* [10]. Since the local homogeneity spheres are preserved by the time evolution, they can be specified by initial conditions such that all the exact fluctuations vanish at r_*: $\mathbf{D}^{(A)}(t, r_*) = 0 \Rightarrow A_q'(t, r_*) = 0$.

In general, sufficient conditions for the existence of extrema can be summarized as follows [10];

(i) If regularity conditions hold, the origin of coordinates is a spatial extremum of the scalars. It will be a minimum (void) if $A_q''(t_0, r = 0) > 0$ or a maximum (overdensity) if $A_q''(t_0, r = 0) < 0$.

(ii) There is a radial extremum of the scalars in the radial interval between two homogeneity spheres: $\Delta_*^i = r_*^{i-1} < r < r_*^i$. This is a maximum or a minimum depending on the sign of $A_q'(t_0, r)$ in Δ_*^i.

(iii) The angular extrema of the scalars lie in the branch $\mathcal{B}_+(r)$ of the curves of angular extrema, while the other branch only contains saddle points.

These extrema are preserved throughout time evolution, pending shell crossings or concavity inversions which we discuss in Sec. III.

C. The dynamics of the models

The dynamics of the models can be fully determined by solving the evolution equations for the variables (7)–(9) (see Appendixes A and B). However, we can also determine the models through their metric functions, in particular the metric function a (which generalizes the Friedman-Lemaître-Robertson-Walker (FLRW) scale factor) follows

from solving the Friedman equation that results from (C8) and (10):

$$t - t_{bb} = \int_0^a \frac{\sqrt{\xi}\,d\xi}{[\frac{8\pi}{3}\rho_{qi} - \mathcal{K}_{qi}\xi + \frac{8\pi}{3}\Lambda\xi^3]^{1/2}}, \quad (16)$$

where $t_{bb} = t_{bb}(r)$ is the inhomogeneous "big-bang time" satisfying $a(t_{bb}(r), r) = 0$, which can be found from evaluating the integral (16) for $t = t_i$ up to $a_i = 1$. The other scale factor Γ in (5) follows by differentiating both sides of (16) and rearranging terms [16]. Once a and Γ are found from the quadrature (16) we have analytic expressions for all relevant variables. If the cosmological constant is neglected, the quadrature (16) is expressible in terms of elementary functions, which leads to analytic solutions of the evolution equations in terms of the scale factors and scaling laws for the q-scalars and their fluctuations. These solutions are given in detail in Appendix B.

Since Szekeres dust models are characterized by all vorticity, 4-acceleration and magnetic Weyl tensor vanishing together, they belong to a class of models called "silent universes" [23,24], in which no information is propagated either by sound or gravitational waves and, consequently, each worldline evolves independently. The quasispherical Szekeres spacetime can be matched either to an FLRW or (de Sitter-)Schwarzschild spacetime [5,11] and due to its silent properties the Szekeres evolution is not affected by our background choice.

III. GRAVITATIONAL COLLAPSE AND VIRIALIZATION

A. Singularities and collapse morphologies

The collapse morphologies can be described through the "expansion tensor" $\mathcal{H}_{ab} = h_a^c h_b^d u_{c;d} = H h_{ab} + \sigma_{ab}$, where h_{ab} and σ_{ab} are the spatial projection and shear tensors, respectively. The tensor $\mathcal{H}_b^a$ admits three eigenvalues:

$$\mathbf{H}_{(1)} = \mathbf{H}_{\parallel} = \frac{\dot{a}}{a} + \frac{\dot{\mathcal{G}}}{\mathcal{G}}, \qquad \mathbf{H}_{(2)} = \mathbf{H}_{(3)} = \mathbf{H}_{\perp} = \frac{\dot{a}}{a}, \quad (17)$$

which follow from expressing this tensor in terms of a canonical orthonormal triad of spacelike unit vectors [23]. Notice that $H = (\mathcal{H}_a^a) = \mathbf{H}_{\parallel} + 2\mathbf{H}_{\perp}$ is a measure of the average expansion/collapse rate. These eigenvalues define three normalized "scale factors" $\{\ell_{(1)}, \ell_{(2)}, \ell_{(3)}\}$ fulfilling $\mathbf{H}_{\parallel} = \dot{\ell}_{\parallel}/\ell_{\parallel}$, $\mathbf{H}_{\perp} = \dot{\ell}_{\perp}/\ell_{\perp}$:

$$\ell_{\parallel} = \ell_{(1)} = a\mathcal{G} = \frac{a(\Gamma - \mathbf{W})}{1 - \mathbf{W}}, \quad (18)$$

$$\ell_{\perp} = \ell_{(2)} = \ell_{(3)} = a, \quad (19)$$

that describe the rate of local expansion/collapse of dust elements along the principal directions, leading to the following collapse morphologies:

Spherical collapse: 3-dimensional collapse in which the three scale factors decrease at a similar rate: $\ell_{(1)}, \ell_{(2)}, \ell_{(3)} \to 0$. For these conditions to occur simultaneously we require $a(r, t_{col}) \to 0$ at the point of collapse.

"Pancake" collapse: 1-dimensional collapse with $\ell_{\parallel} \to 0$ or decreasing close to zero and $\mathbf{H}_{\parallel}$ becoming very small or negative, with $\ell_{\perp} \gg \ell_{\parallel}$.

Filamentary collapse: Collapse along two principal directions, hence: $\ell_{\perp} \to 0$ with finite (or diverging) $\ell_{\parallel}$.

B. Shell crossings singularities and concavity inversions

1. Shell crossings singularities

These singularities occur when the mass density diverges as the proper distance between comoving layers (with different comoving coordinates r) vanishes, while their area distances $R = ar$ remain greater than zero. Shell crossings are considered weak singularities or less severe than the big bang or big crunch (which occur as $a \to 0$), and they can be transformed away by a continuous nondifferentiable (C^0) coordinate transformation [5,25,26].

Shell crossings singularities can be avoided throughout the evolution of dust layers by suitable choices of the initial data. In Szekeres models the necessary and sufficient condition to prevent shell crossings can be simply stated as

$$\Gamma - \mathbf{W} > 0 \quad \text{for all } (t, \vec{r}) \text{ such that } a > 0. \quad (20)$$

For the case $\Lambda = 0$ condition (20) can be expressed in terms of the initial functions, but for the general case with $\Lambda > 0$ the fulfilment of this condition must be verified numerically (see Appendix D).

The emergence of shell crossings (i.e. caustics) mark the onset of virialization processes (phase mixing and violent relaxation) characteristic of collisionless systems (whether cold dark matter WIMP's or baryons), which indicates the breaking down of a dust continuum as an idealized matter-energy model [20,27]. Nevertheless, we emphasize that the dynamical description that we have provided of the formation of pancake-like structures from the Szekeres dust models (connected to the Zeldovich approximation [17]) is appropriate up to the emergence of these caustics. The proper description of the dynamics of structure formation beyond these caustics lies beyond the present paper and can be obtained (albeit approximately) by numerical N-body simulations, see Sec. 4. 10. 3 of [27] for details. In the following we explore the conditions to obtain an evolution free from shell crossings, or at least for shell crossings forming sufficiently close to the big crunch so that they are covered and hidden away by an apparent horizon.

TABLE I.   All possible cases for the evolution of a dust shell occupying the region $(r_1^* < r < r_2^*)$ in LTB/Szekeres with $\Lambda = 0$. The table shows the signs of the radial derivative of the big bang and collapse times as well as the sign of the density fluctuation as we approach the big crunch. Although positive signs of t'_{bb} and negative signs of t'_{coll} necessarily lead to shell crossings, the shell crossings produced by $t'_{bb} > 0$ occur before t_i, out of the range of validity of the model.

Cases	Description[a]		Sign(t'_{bb})	Sign(t'_{coll})	Sign($D^{(\rho)}_{coll}$)
I	$\delta_0^{(\beta)} = 0$ $(\delta_0^{(\beta)} = -\frac{3}{2}\delta_0^{(\mathcal{K})})$		$-$Sign($\delta_0^{(\mathcal{K})}$)	$-$Sign($\delta_0^{(\mathcal{K})}$)	Sign($\delta_0^{(\mathcal{K})}$)
II	$\delta_0^{(\mathcal{K})} = 0$ $(\delta_0^{(\beta)} = \delta_0^{(\rho)})$		Sign($\delta_0^{(\rho)}$)	Sign($\delta_0^{(\rho)}$)	$-$Sign($\delta_0^{(\rho)}$)
III	$\delta_0^{(\beta)} = 0$		Sign($\delta_0^{(\rho)}$)	Sign($\delta_0^{(\rho)}$)	$-$Sign($\delta_0^{(\rho)}$)
IV[b]	$t'_{bb} < 0$	$\delta_0^{(\beta)} < 0$	-1	-1	± 1
		$\delta_0^{(\beta)} > 0$	-1	± 1	± 1
V[b]	$t'_{bb} = 0$	$\delta_0^{(\beta)} < 0$	0	-1	$+1$
		$\delta_0^{(\beta)} > 0$	0	$+1$	-1
VI[b]	$t'_{bb} > 0$	$\delta_0^{(\beta)} < 0$	$+1$	-1	$+1$
			$+1$	$+1$	-1
		$\delta_0^{(\beta)} > 0$	$+1$	$+1$	-1

[a]$\delta_0^{(\beta)} \equiv \delta_0^{(\rho)} - \frac{3}{2}\delta_0^{(\mathcal{K})}$.

[b]$\delta^{(\rho)}$, $\delta_0^{(\mathcal{K})}$ and $\delta_0^{(\beta)} \neq 0$.

2. Concavity inversions

The concavity associated with an inhomogeneity (whether density has the local shape of a "clump" or "void") is closely related with the local sign of the "radial" coordinate derivatives $(\partial/\partial r)$ of the density, which is in turn related with the local sign of the density fluctuation $\Delta^{(\rho)}$. Hence, a local maximum (minimum) in ρ will indicate both a upward (downward) local concave profile and an overdensity (underdensity or void). Since the density fluctuation can change its sign along the time evolution of the model, local concavity inversions (from clumps to voids or vice versa) can occur indicating that local maxima evolve into local minima and vice versa. The conditions for these local concavity inversions follow from the existence of solutions of $D^{(\rho)} = 0$ (or $\Delta^{(\rho)} = 0$):

$$D^{(\rho)} = 0 \Leftrightarrow H_{qi}(\Psi_q - \Psi_{qi}) + \frac{2}{3}\left(1 - \frac{H_{qi}}{H_q}\right) = -\frac{\delta_i^{(\rho)}}{3(\delta_i^{(\rho)} - \frac{3}{2}\delta_i^{(\mathcal{K})})},$$
(21)

with $\Psi_q = H_q(t - t_{bb})$. As shown in [28] for the central extremum in generic LT models, the presence of a decaying mode, or equivalently a nonhomogeneous big-bang time [29], is a required condition for this phenomenon (a statement that is also valid for the evolution of a thick dust shell).

In Table I we examine the possible concavity inversions and shell crossings in the evolution of a dust shell for the case $\Lambda = 0$. By looking at all possible combinations of initial conditions, we find that it is impossible to have an evolution of overdensities that keep the original concavity

profile and collapse onto a BH (a big crunch central singularity) without shell crossings at late times.[3] That is, the collapse to a big crunch singularity will take place only if the original overdensity is inverted into a void, directly associated to the decaying mode. (See Fig. 1 for an illustration of this aspect.)

C. Apparent horizon

The apparent horizon is the surface boundary of the region containing trapped surfaces in which outgoing null geodesic congruences present a negative expansion scalar. Although some "new effects" appear in quasi-spherical Szekeres models due to the lack of symmetry [5,6,15,30], this definition results in the same condition as in LTB models: $R = 2M$ [31]. Further, in the matching with a Schwarzschild exterior the apparent horizon thus defined coincides with the Schwarzschild event horizon.[4]

IV. SETTING UP MODELS OF MULTIPLE COLLAPSING STRUCTURES

We consider the multiple collapse of cold dark matter structures, with each structure defined by a density maximum of quasispherical Szekeres or LTB dust models. Such configurations are obtained via a smooth matching along the homogeneities spheres of sections of distinct Szekeres

---

[3]Shell crossings at very early times (i.e. before t_i) are not problematic since they occur out of the range of applicability of the model.

[4]Note that since the apparent horizon is a quasilocal and foliation-dependent concept, we could have employed another criterium for BH formation instead of the surface $R = 2M$, e.g. a concept based on scalar curvature invariants is proposed in [32].
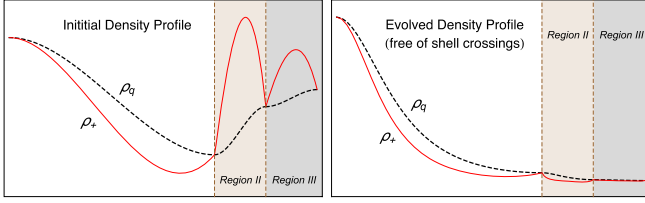
FIG. 1. Comparison of density profiles. The panels show the profile of the mass density $\rho(r, t, \theta)$ evaluated along the curve of the angular maxima of **W** (red and solid) and the q-density average $\rho_q(r, t)$ [black and dotted, Eq. (7)]. The left panel shows a typical initial setup of multiple overdensity structures. Evolved with the growing mode, the Szekeres regions II and III will eventually present shell crossings. On the other hand, the right panel shows the evolution with a dominant decaying mode which flattens the profile and allows for a collapse free of shell crossings (at least at late times).

spacetimes, and constitute global self-consistent exact solutions of Einstein's equations, as long as the Darmois matching conditions are satisfied along the interfaces of the sections [17,33–38].

We look at a specific configuration consisting of a central spherical overdensity described by a section of an LTB spacetime, surrounded by two Szekeres shells, each one hosting a nonspherical overdensity, with the most external one smoothly matched to a Schwarzschild exterior. By taking the dipole parameter $Y = Z = 0$ and $X \neq 0$, the angular location of these nonspherical overdensities is set at $\phi = 0$ and $\theta = \pi/2$ (x axis; see e.g. Fig. 2).

The initial density mass is given in terms of a dimensionless q-density function (μ_q) defined as follows:

$$[\mu_q(\chi)]_i = \frac{4\pi[\rho_q]_i}{3H_*^2}, \quad \text{with} \quad \chi = r/l_s, \qquad (22)$$

where l_s and H_* are the characteristic length scale and the inverse of the characteristic time scale, respectively. In
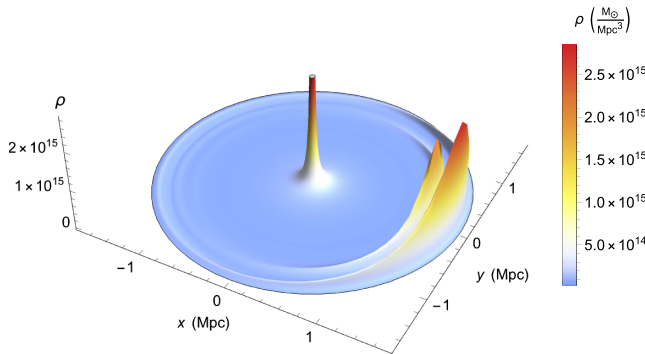

FIG. 2. Density mass in the equatorial plane in units of $M_\odot/\text{Mpc}^3$. Equatorial projection of the density mass distribution at a time close, but before to the time of shell crossings. The "x" and "y" axes respectively correspond to $R\cos\phi$ and $R\sin\phi$, with $R = ar$.

TABLE II. Initial conditions. The table displays the piecewise definition of the functions μ_{qi} and **W** needed to either integrate the system (C2)–(C9) or evaluate the analytic solutions shown in B. Functions $\mathcal{Q}_i$ are third order polynomials defined by their values and vanishing first derivatives at $\chi_*^0, \chi_*^1, \chi_*^2$ and χ_*^3. k_2 and k_3 are the amplitude constants of the dipole magnitude.

	$0 < \chi < \chi_*^1$	$\chi_*^1 < \chi < \chi_*^2$	$\chi_*^2 < \chi < \chi_*^3$
μ_{qi}	$\mathcal{Q}_1(\chi)$	$\mathcal{Q}_2(\chi)$	$\mathcal{Q}_3(\chi)$
W	$X = Y = Z = 0$	$X = -k_2 \times$ $\times \sin^2\left(\frac{\chi-\chi_*^1}{\chi_*^2-\chi_*^1}\pi\right)$ $Y = Z = 0$	$X = -k_3 \times$ $\times \sin^2\left(\frac{\chi-\chi_*^2}{\chi_*^3-\chi_*^2}\pi\right)$ $Y = Z = 0$

addition, we define the dimensionless curvature ($\kappa_q = \mathcal{K}_q/H_*^2$) and rewrite the evolution equations, as well as their analytic solutions, in terms of dimensionless quantities. Proceeding along these lines we have the freedom of choice for both temporal and spatial scales. As a consequence a single numerical solution can have various interpretations, corresponding to different evolution times [$t - t_{\text{bb}} = (\tau - \tau_{\text{bb}})/H_*$] and length scales [$R(\tau, \chi) = \chi a(\tau, \chi) l_s$].

Furthermore, we impose initial conditions with a homogeneous big-bang time ($t'_{\text{bb}} = 0$), which sets the initial q-curvature through Eq. (B3). This widely used condition is equivalent to avoiding the decaying modes [29].

We find that it is impossible to follow the full evolution of collapsing overdensities without shell crossings emerging before the big crunch. Therefore, we have no alternative but to allow for their presence. In the following we present two possible outcomes from the choice of time and length scales, which result in two different astrophysical objects. The initial conditions for these two scenarios are listed in Table II.

A. An approximate model for a galaxy cluster

As a first case, we examine the evolution of a multiple structures configuration from linear conditions at a redshift $z = 7$ to a present day final configuration of scale ~ 1 Mpc and mass of $\sim 10^{15} M_\odot$, which can be compared to a galactic super–cluster[5] In general terms the evolution proceeds as follows, the structures are initially expanding, then reach (not simultaneously) the turnaround point. Subsequently, at the present cosmic time, when the shell crossings first appear, part of the central structure has already collapsed into a hidden spherical singularity. Considering the shell crossings as rough estimators of

---

[5]Following the scheme of Table II, we set $\mathcal{Q}_1(0) = 1 + 9.1 \times 10^{-3}$, $\mathcal{Q}_1(\chi_*^1) = \mathcal{Q}_2(\chi_*^1) = 1 + 10^{-3}$, $\mathcal{Q}_2(\chi_*^2) = \mathcal{Q}_3(\chi_*^2) = 1 + 2 \times 10^{-3}$ and $\mathcal{Q}_3(\chi_*^3) = 1 + 3 \times 10^{-3}$ for the piecewise polynomial, $k_1 = 5.5 \times 10^{-1}$ and $k_2 = 3.4 \times 10^{-1}$ for the dipole magnitude and the constant $H_* = 2/(3t_{z=7})$.
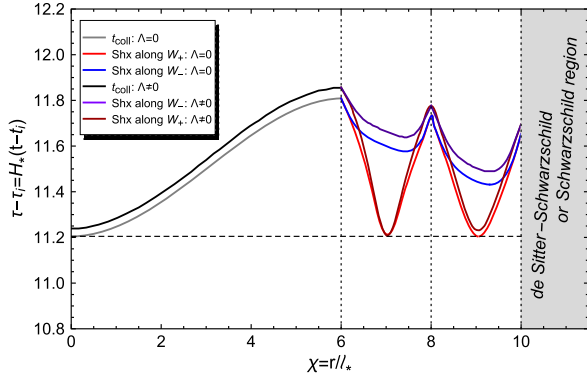
FIG. 3. Collapse and shell crossings times. Grey, light red and blue curves respectively represent the times of collapse and shell crossing along the direction of the maxima and minima of the dipole for the case $\Lambda = 0$. Black, dark red and violet lines respectively represent the time of collapse and shell crossings considering Λ.
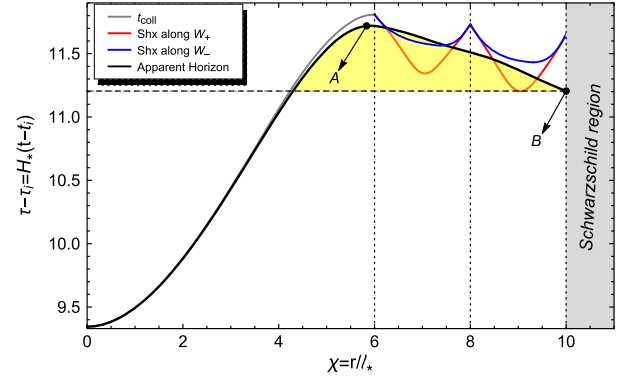

FIG. 4. Hiding the shell crossing singularities behind the apparent horizon surface. The apparent horizon (black curve) hides the shell crossings thus they are already inside the black hole by the time they appear. Notice that in the yellow-shaded area the apparent horizon first appears at the point B, where t_{AH} has a local minimum, $t_{AH}^{(B)}$. At all times in the interval $(t_{AH}^{(B)}, t_{AH}^{(A)})$, the mass swallowed up by the singularity is necessarily smaller than the mass into the AH.

the virialization time (as interpreted in Sec. III B 1), we can argue that the whole set of structures correspond to a cluster that is virializing today and hosting a central BH of $\sim 10^9 \ M_\odot$ (see Fig. 2).

The times of collapse and shell crossings are shown in Fig. 3. While the collapse time only depends on the comoving radial coordinate, the shell crossing time depends on all the spatial coordinates [cf. Eq. (20)]. The red and blue curves represent the shell crossings times along the curves of angular maxima and minima of the dipole function, respectively. We also plot the results of the calculations taking into account the cosmological constant, whose sole effect is to delay the collapse and the shell crossings.

B. A model for multiple collapse into a black hole

Another choice is to delay the shell crossings as much as possible (i.e. as close as possible to the big crunch) and accumulate enough mass as to cover them within an apparent horizon surface. For that purpose, at the time when shell crossings emerge (τ_{Shx}) the apparent horizon radius must satisfy,

$$[R(\tau, \chi) = 2M(\chi)]_{(\tau_{Shx}, \chi_*^3)}, \tag{23}$$

where $R = a\chi l_s$ is the area distance, $M = (4\pi/3)\rho_{qi}(\chi l_s)^3$ is the quasilocal mass of the whole configuration and χ_* marks the boundary between the Szekeres and Schwarzschild regions. At this surface the apparent horizon coincides with the Schwarzschild event horizon, so by construction, we will have a covered singularity.[6] Figure 4

depicts the collapse and shell crossing times, as well as the apparent horizon curve covering the shell crossing singularities. However, the fulfilment of the condition (23) demands either extremely large values of the overall mass or very short collapse times. To illustrate this we consider as a first example a case with initial conditions at $z = 7$ such that the shell crossings appeared approximately today. Then after undertaking an extensive search of initial conditions, by trial and error we found that hiding the shell crossing inside the apparent horizon requires large total masses of the order of $10^{20} \ M_\odot$. As shown in the left panel of Fig. 5, for mass values of astrophysical or galactic BHs the shell crossings are formed before being covered by the apparent horizon. The red-shaded area represents the values of time/mass for which the shell crossings remain uncovered. Conversely one can impose, instead of a fixed shell crossing time, a final mass for the apparent horizon $M = M_{BH}$. Equation (23) thus fixes the time and length scales for the BH formation. With this choice we find that, just as for the case of PBH formation, the timescales for the collapse are very short (as shown in right panel of Fig. 5). For instance, a typical supermassive BH ($M \approx 10^9 \ M_\odot$) would collapse in less than a year ($t_{col} - t_i \approx 0.005$ yr), while a PBH formed in an early dust-like era at the reheating period is allowed to present a mass of order $M \approx 10^{-16} \ M_\odot$ [39], and our results show a time of collapse of order $t_{col} - t_i \approx 10^{-20}$ s. This is in agreement with numerical simulations of PBH formation [40].

So far we have been concerned with the collapse of multiple pancake-shaped overdensities whose evolution cannot avoid the appearance of shell crossings. The shell crossings, however, can be avoided (at least at later times) by choosing initial conditions whose evolution exhibits

---

[6]We took $\mathcal{Q}_1(0) = 1 + 4 \times 10^{-2}$, $\mathcal{Q}_1(\chi_*^1) = \mathcal{Q}_2(\chi_*^1) = 1 + 10^{-3}$, $\mathcal{Q}_2(\chi_*^2) = \mathcal{Q}_3(\chi_*^2) = 1 + 2 \times 10^{-3}$ and $\mathcal{Q}_3(\chi_*^3) = 1 + 3 \times 10^{-3}$, $k_1 = 4 \times 10^{-1}$, $k_2 = 3.4 \times 10^{-1}$ and the constant $H_* = 2/(3t_{z=7})$ (see Table II).
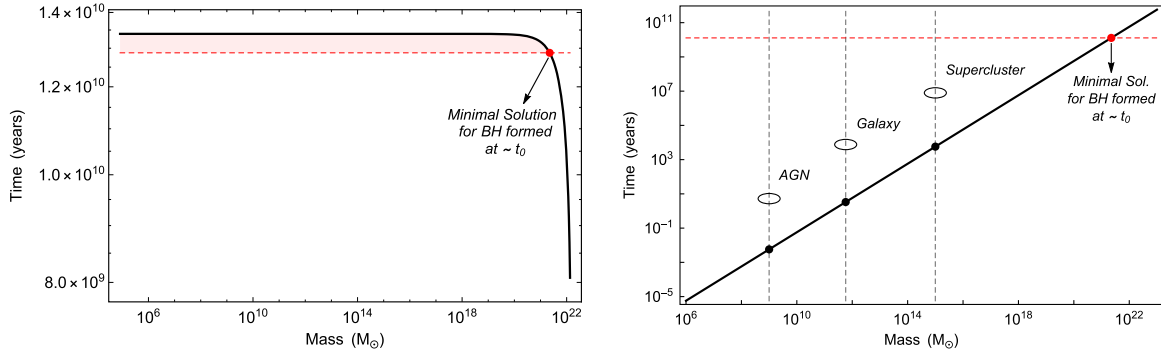
FIG. 5.   Black hole formation time as function of the mass. The left panel shows with a black line the time in which the entire region of Szekeres has been hidden behind the apparent horizon as a function of black hole mass. For the values of time and masses shaded in red, which include the masses of astrophysical black holes, the shell crossings are formed outside the apparent horizon. The curve in the right panel represents the collapse time as a function the of the mass demanding the condition (23) to be satisfied. We have also indicated with dashed grey lines the typical masses of active galactic nuclei (AGN, $\sim 10^9$ $M_\odot$), galaxies ($\sim 10^{11}$ $M_\odot$) and superclusters ($\sim 10^{15}$ $M_\odot$), as a reference.

concavity inversions which can complete the collapse of dust overdensities towards the central singularity. The resulting mass distribution exhibits a collapse that is qualitatively analogous to that of collapsing LTB models (see Fig. 1) but is sourced by configurations that evolve away of the pure growing mode.

V. DISCUSSION AND FINAL REMARKS

In this paper we have studied the collapse of nonspherical structures, modeled by multiple concentrations of pressureless matter. We have examined an interesting type of collapse through the joint evolution of a central spherical overdensity and neighbor nonspherical structures. Specifically, we have looked at the formation of a spherical apparent horizon, and characterised the possible shell crossings that prevent BH formation. The latter are interpreted as the breakdown of the dust model and the onset of an intricate virialization process beyond the Szekeres description [20].

We have found that the conditions to prevent shell crossings are much more stringent in regions that deviate significantly from homogeneity [cf. condition (20)]. Specifically, we have shown that shell crossings cannot be avoided in the collapse of regions where high density pancake-like inhomogeneities evolve in the pure growing mode. One way of interpreting the evolution of these multiple configurations is to consider the shell crossings as the onset of virialization. Note that this characteristic is not exclusive of the nonspherical collapse, since the reported general conditions for the formation of shell crossings (in Table I) hold even for the case where the dipole is null (LTB case).

In Sec. IV A, we exemplify the evolution of a galaxy cluster which starts at $z = 7$ up until the present cosmic time. We simulate the formation of both a central back hole of mass $M \sim 10^9$ $M_\odot$, and a couple of overdensities which

evolve up to the shell crossing time (interpreted as the start of virialization of galaxy components).

To examine a full collapse of multiple configurations we have presented examples where the initial conditions delay the emergence of shell crossings, so that the latter are covered by an apparent horizon, and remain undetectable to observers in the exterior Schwarzschild spacetime. In this case, the fact that some dust layers terminate at a shell crossings is practically indistinguishable from the "real" collapse in which they terminate at the central singularity.

The fine-tuned initial conditions needed to build such configuration, impose constraints on the BH mass and collapse time of the whole structure which are incompatible with astrophysical scales. For example, considering masses of the size of a galactic system we find that extremely large density concentrations are required to obtain a final single BH in an astrophysical and/or cosmological time scales, see Fig. 4. If we assume an initial time around $z \sim 7$, as in our example, the initial distribution of inhomogeneities of galactic mass collapses completely to form a BH of the order of 10^{20} $M_\odot$, which is at least 5 orders of magnitude larger than the typical supercluster mass.

Alternatively, if we wish to impose a smaller mass for the BH to coincide with (say) a large massive BH in the center of a galaxy ($M \sim 10^9$ $M_\odot$), then the collapsing timescales become extremely small ($t_{col} \sim 0.005$ yr, see right panel of Fig. 5). As a consequence, the collapse of nonspherical dust configurations is not an appropriate mechanism to form BHs of astrophysical interest (stellar size or massive BHs in galactic centres or AGNs), not even as a rough toy model level.

It is not surprising that self-consistent astrophysical BHs formed from the collapse of nonspherical pancake structures are prevented by shell crossings, as these BHs form from rotating baryonic sources in which hydrodynamical processes become dominant in the regime near the collapse.

On the other hand, BH formation in the type of Szekeres configurations we are considering is consistent with PBHs formation scenarios that involve much smaller masses and very fast collapsing times. For example, a PBH formed in an early dust-like era of mass $M \approx 10^{-16} \, M_{\odot}$, would collapse in $\sim 10^{-20}$ seconds. This is perfectly consistent with PBH formation timescales and our result may complement previous work assessing the formation of PBHs in an early dust-like era [39,41–43]. Our result also argues in favor of recent work on the formation of PBHs from nonspherical configurations [14,22].

Finally we comment on the flexibility of the featured model. Our results present enough freedom as to set the mass as an initial condition and preserve it throughout the evolution. Additionally we can manipulate the parameters to set shell crossing times for nonspherical overdensities. This freedom allows us to model either a multiple structures collapse (as in the last case studied in Sec. IV B, and on the other hand, allowing for the concavity inversion of inhomogeneities, we can follow their evolution without shell crossing singularities up to the time when they cross the apparent horizon. All the freedom of our model is manifest when working with dimensionless quantities.

APPENDIX A: EVOLUTION EQUATIONS FOR NUMERICAL WORK

The models become fully determined by solving numerically the following set of first order autonomous partial differential equations (which are effectively constrained ordinary differential equations):

$$\dot{\rho}_q = -3\rho_q \mathcal{H}_q, \tag{A1}$$

$$\dot{H}_q = -H_q^2 - \frac{4\pi}{3}\rho_q + \frac{8\pi}{3}\Lambda, \tag{A2}$$

$$\dot{\Delta}^{(\rho)} = -3(1 + \Delta^{(\rho)})\mathbf{D}^{(H)} \tag{A3}$$

$$\dot{\mathbf{D}}^{(H)} = (-2H_q + 3\mathbf{D}^{(H)})\mathbf{D}^{(H)} - \frac{4\pi}{3}\rho_q \Delta^{(\rho)}, \tag{A4}$$

$$\dot{a} = aH_q, \tag{A5}$$

$$\dot{\mathcal{G}} = 3\mathcal{G}\mathbf{D}^{(H)}, \qquad \mathcal{G} = \frac{\Gamma - \mathbf{W}}{1 - \mathbf{W}}, \tag{A6}$$

subject to the algebraic constraints:

$$H_q^2 = \frac{8\pi}{3}[\rho_q + \Lambda] - \mathcal{K}_q, \tag{A7}$$

$$\frac{3}{2}\mathbf{D}^{(\mathcal{K})} = 4\pi\rho_q \Delta^{(\rho)} - 3H_q \mathbf{D}^{(H)}, \tag{A8}$$

where the q scalars A_q and their fluctuations, $\mathbf{D}^{(A)}$ and $\Delta^{(\rho)}$, are defined in Sec. II A.

APPENDIX B: ANALYTIC SOLUTIONS FOR $\Lambda = 0$

For elliptic models, $K > 0$, the solution of the quadrature (16) is given explicitly as follows (see [16] for more details and solutions for parabolic and hyperbolic models):

$$t - t_{\text{bb}} = \begin{cases} \mathcal{F}_e(\alpha_q)/\beta_{qi} & \text{expanding phase } H_{qi} > 0, \\ [2\pi - \mathcal{F}_e(\alpha_q)]/\beta_{qi} & \text{collapsing phase } H_{qi} < 0, \end{cases} \tag{B1}$$

where $\alpha_q = \alpha_{qi}a$, $\alpha_{qi} = \frac{3}{4\pi}|\mathcal{K}_{qi}|/\rho_{qi}$, $\beta_{qi} = \frac{3}{4\pi}|\mathcal{K}_{qi}|^{3/2}/\rho_{qi}$ and $\mathcal{F}_e$ is defined as

$$\mathcal{F}_e = u \mapsto \arccos(1 - u) - \sqrt{u}\sqrt{2 - u}. \tag{B2}$$

The big bang, maximal expansion and collapsing times are given by

$$t_{\text{bb}} = t_i - \frac{\mathcal{F}_e(\alpha_{qi})}{\bar{H}_* \beta_{qi}}, \qquad t_{\text{max}} = t_{\text{bb}} + \frac{\pi}{H_* \beta_{qi}},$$
$$t_{\text{coll}} = t_{\text{bb}} + \frac{2\pi}{H_* \beta_{qi}}, \tag{B3}$$

and the expression for the metric function Γ, obtained from (B1), takes the following form:

$$\Gamma = 1 + \delta_i^{(\rho)} - 3\left(\delta_i^{(\rho)} - \frac{3}{2}\delta_i^{(\mathcal{K})}\right)\left[\Psi_q - \frac{2}{3}\right] - H_q r t'_{\text{bb}}, \tag{B4}$$

with H_q, Ψ_q, $\delta_i^{(\rho)}$ and $\delta_i^{(\mathcal{K})}$ given by

$$H_q = \frac{\dot{a}}{a} = \pm \frac{\sqrt{\frac{4\pi}{3}\rho_{qi}}\sqrt{2 - \alpha_q}}{a^{3/2}}, \tag{B5}$$

$$\Psi_q(\alpha_q) \equiv H_q(t - t_{\text{bb}}) = \frac{H_q}{\bar{H}_*}\frac{\mathcal{F}(\alpha_q)}{\beta_{qi}} \tag{B6}$$

$$\delta_i^{(\rho)} = \Delta_i^{(\rho)}|_{\mathbf{W}=0} = \frac{r}{3}\frac{\rho'_{qi}}{\rho_{qi}}, \tag{B7}$$

$$\delta_i^{(\mathcal{K})} = \Delta_i^{(\mathcal{K})}|_{\mathbf{W}=0} = \frac{r}{3}\frac{\mathcal{K}'_{qi}}{\mathcal{K}_{qi}}. \tag{B8}$$

For the analysis of the existence of shell crossings, it is worthwhile to rewrite Γ in the following form, valid during the collapsing phase ($H_q < 0$):

$$\Gamma = 1 + \delta_i^{(\rho)} - 3\left(\delta_i^{(\rho)} - \frac{3}{2}\delta_i^{(\mathcal{K})}\right)\left[|H_q(t - t_{\text{coll}})| - \frac{2}{3}\right]$$
$$+ |H_q|rt'_{\text{coll}}. \tag{B9}$$

APPENDIX C: DIMENSIONLESS EVOLUTION EQUATIONS AND ANALYTIC SOLUTIONS

By introducing dimensionless time, $\tau = H_* t$, scale, $R_i = r = \chi l_s$, and variables,

$$\mu_q = \frac{4\pi}{3}\frac{\rho_q}{H_*^2}, \qquad \kappa_q = \frac{\mathcal{K}_q}{H_*^2}, \qquad h_q = \frac{H_q}{H_*^2}, \qquad \lambda = \frac{8\pi}{3}\Lambda, \tag{C1}$$

the evolution equations result in the following dimensionless system:

$$\dot{\mu}_q = -3\mu_q\mathcal{H}_q, \tag{C2}$$

$$\dot{h}_q = -h_q^2 - \mu_q + \lambda, \tag{C3}$$

$$\dot{\Delta}^{(\mu)} = -3(1 + \Delta^{(\mu)})\mathbf{D}^{(h)} \tag{C4}$$

$$\dot{\mathbf{D}}^{(h)} = (-2h_q + 3\mathbf{D}^{(h)})\mathbf{D}^{(h)} - \mu_q\Delta^{(\mu)}, \tag{C5}$$

$$\dot{a} = ah_q, \tag{C6}$$

$$\dot{\mathcal{G}} = 3\mathcal{G}\mathbf{D}^{(h)}, \qquad \mathcal{G} = \frac{\Gamma - \mathbf{W}}{1 - \mathbf{W}}, \tag{C7}$$

subject to the constraints:

$$h_q^2 = 2\mu_q + \lambda - \kappa_q, \tag{C8}$$

$$\frac{1}{2}\mathbf{D}^{(\kappa)} = \mu_q\Delta^{(\mu)} - h_q\mathbf{D}^{(h)}, \tag{C9}$$

where the arbitrary constants H_* and l_s set the time and spatial scales, respectively. As above, $\mathbf{D}^{(A)} = A - A_q$ denotes the exact fluctuations and $\Delta^{(\mu)} = (\mu - \mu_q)/\mu_q$.

On the other hand the analytic solution for the case with $\Lambda = 0$, Eq. (C10), can be rewritten in terms of dimensionless quantities as

$$\tau - \tau_{\text{bb}} = \begin{cases} \mathcal{F}_e(\hat{\alpha}_q)/\hat{\beta}_{qi} & \text{expanding phase } h_{qi} > 0, \\ [2\pi - \mathcal{F}_e(\hat{\alpha}_q)]/\hat{\beta}_{qi} & \text{collapsing phase } h_{qi} < 0, \end{cases} \tag{C10}$$

where $\hat{\alpha}_q = \hat{\alpha}_{qi}a$, $\hat{\alpha}_{qi} = |\kappa_{qi}|/\mu_{qi}$, $\hat{\beta}_{qi} = |\kappa_{qi}|^{3/2}/\mu_{qi}$ and $\mathcal{F}_e$ was defined above in Eq. (B2). Further, the

dimensionless big bang, maximal expansion and collapsing times are given by

$$\tau_{\text{bb}} = \tau_i - \frac{\mathcal{F}_e(\hat{\alpha}_{qi})}{\hat{\beta}_{qi}}, \qquad \tau_{\text{max}} = \tau_{\text{bb}} + \frac{\pi}{\hat{\beta}_{qi}},$$

$$\tau_{\text{coll}} = \tau_{\text{bb}} + \frac{2\pi}{\hat{\beta}_{qi}}, \tag{C11}$$

and the expression for the metric function Γ reads

$$\Gamma = 1 + \delta_i^{(\mu)} - 3\left(\delta_i^{(\mu)} - \frac{3}{2}\delta_i^{(\kappa)}\right)\left[\hat{\Psi}_q - \frac{2}{3}\right] - h_q\chi\tau'_{\text{bb}}, \tag{C12}$$

where

$$h_q = \frac{\dot{a}}{a} = \pm\frac{\sqrt{\mu_{qi}}\sqrt{2 - \hat{\alpha}_q}}{a^{3/2}}, \tag{C13}$$

$$\hat{\Psi}_q(\hat{\alpha}_q) \equiv h_q(\tau - \tau_{\text{bb}}) = h_q\frac{\mathcal{F}(\hat{\alpha}_q)}{\hat{\beta}_{qi}} \tag{C14}$$

$$\delta_i^{(\mu)} = \Delta_i^{(\mu)}|_{\mathbf{W}=0} = \frac{\chi}{3}\frac{\mu'_{qi}}{\mu_{qi}}, \tag{C15}$$

$$\delta_i^{(\kappa)} = \Delta_i^{(\kappa)}|_{\mathbf{W}=0} = \frac{\chi}{3}\frac{\kappa'_{qi}}{\kappa_{qi}}. \tag{C16}$$

APPENDIX D: AVOIDANCE OF SHELL CROSSINGS

The necessary and sufficient condition to avoid shell crossings can be simply stated as

$$\Gamma - \mathbf{W} > 0 \quad \text{for all } (t, \vec{r}) \text{ such that } a > 0. \tag{D1}$$

From this equation we obtain various necessary (but not sufficient) conditions, such as $\Gamma > 0$, $|\mathbf{W}| < 1$, $0 < X^2 + Y^2 + Z^2 < 1$ and $|X|, |Y|, |Z| < 1$. For the general case $\Lambda > 0$ the necessary and sufficient condition (D1) must be verified numerically, but for the case $\Lambda = 0$ it can be given in terms of initial value functions. For elliptic models (or regions) these conditions are summarized as follows [16]

$$1 + \delta_i^{(\rho)} - \mathbf{W} \geq 0, \qquad t'_{\text{bb}} \leq 0, \qquad t'_{\text{coll}} \geq 0, \tag{D2}$$

$$\delta_i^{(\rho)} - \frac{3}{2}\delta_i^{(\mathcal{K})} \geq 0 \quad \text{necessary not sufficient.} \tag{D3}$$

Notice that for the study of a collapsing region the condition $t'_{\text{bb}} \leq 0$ can be relaxed, as it would produce shell crossings that can be confined to early cosmic times if rt'_{bb} is much smaller than horizon distances at $t = t_i$.

[1] B. Datt, Z. Phys. **108,** 314 (1938); J. R. Oppenheimer and H. Snyder, Phys. Rev. **56,** 455 (1939); B. Waugh and K. Lake, Phys. Rev. D **38,** 1315 (1988); P. Joshi and I. Dwivedi, Phys. Rev. D **47,** 5357 (1993); P. S. Joshi, N. Dadhich, and R. Maartens, Phys. Rev. D **65,** 101501 (2002); P. S. Joshi and D. Malafarina, Classical Quantum Gravity **32,** 145004 (2015); D. M. Eardley and L. Smarr, Phys. Rev. D **19,** 2239 (1979); D. Christodoulou, Commun. Math. Phys. **93,** 171 (1984); R. P. Newman, Classical Quantum Gravity **3,** 527 (1986); P. Joshi and I. Dwivedi, Commun. Math. Phys. **146,** 333 (1992); I. Dwivedi and P. Joshi, Commun. Math. Phys. **166,** 117 (1994); G. Magli, Classical Quantum Gravity **14,** 1937 (1997); **15,** 3215 (1998); T. Harada, Phys. Rev. D **58,** 104015 (1998); T. Harada, K.-i. Nakao, and H. Iguchi, Classical Quantum Gravity **16,** 2785 (1999); J. F. V. da Rocha and A. Wang, Classical Quantum Gravity **17,** 2589 (2000); T. Harada and H. Maeda, Phys. Rev. D **63,** 084022 (2001); R. Goswami and P. S. Joshi, Classical Quantum Gravity **19,** 5229 (2002); S. M. Goncalves, S. Jhingan, and G. Magli, Phys. Rev. D **65,** 064011 (2002); R. Giambo, F. Giannoni, G. Magli, and P. Piccione, Commun. Math. Phys. **235,** 545 (2003); Gen. Relativ. Gravit. **36,** 1279 (2004); R. Goswami and P. S. Joshi, Classical Quantum Gravity **21,** 3645 (2004); S. Satin, D. Malafarina, and P. S. Joshi, Int. J. Mod. Phys. D **25,** 1650023 (2016).

[2] P. S. Joshi and D. Malafarina, Int. J. Mod. Phys. D **20,** 2641 (2011).

[3] C. Gundlach and J. M. Martín-García, Living Rev. Relativity **10,** 5 (2007).

[4] A. Krasinski, *Inhomogeneous Cosmological Models* (Cambridge University Press, Cambridge, 1997).

[5] J. Plebanski and A. Krasinski, *An Introduction to General Relativity and Cosmology* (Cambridge University Press, Cambridge, 2006).

[6] K. Bolejko, A. Krasiński, C. Hellaby, and M.-N. Célérier, *Structures in the Universe by Exact Methods: Formation, Evolution, Interactions* (Cambridge University Press, Cambridge, 2009).

[7] K. Bolejko, Phys. Rev. D **73,** 123508 (2006).

[8] K. Bolejko, Phys. Rev. D **75,** 043508 (2007).

[9] K. Bolejko and R. A. Sussman, Phys. Lett. B **697,** 265 (2011).

[10] R. A. Sussman and I. D. Gaspar, Phys. Rev. D **92,** 083533 (2015).

[11] C. Hellaby and A. Krasinski, Phys. Rev. D **77,** 023529 (2008).

[12] A. Walters and C. Hellaby, J. Cosmol. Astropart. Phys. 12 (2012) 001.

[13] A. Krasinski, Phys. Rev. D **78,** 064038 (2008); **85,** 069903(E) (2012); M. Ishak, J. Richardson, D. Whittington, and D. Garred, Phys. Rev. D **78,** 123531 (2008); **84,** 089902(E) (2011); K. Bolejko, Gen. Relativ. Gravit. **41,** 1737 (2009); K. Bolejko and M.-N. Celerier, Phys. Rev. D **82,** 103510 (2010); A. Krasinski and K. Bolejko, Phys. Rev. D **83,** 083503 (2011); A. Nwankwo, M. Ishak, and J. Thompson, J. Cosmol. Astropart. Phys. 05 (2011) 028; M. Ishak and A. Peel, Phys. Rev. D **85,** 083502 (2012); A. Peel, M. Ishak, and M. A. Troxel, Phys. Rev. D **86,** 123508 (2012); M. Ishak, A. Peel,

and M. A. Troxel, Phys. Rev. Lett. **111,** 251302 (2013); S. M. Koksbang and S. Hannestad, Phys. Rev. D **91,** 043508 (2015); **92,** 023532 (2015); **92,** 069904(E) (2015); K. Bolejko, M. A. Nazer, and D. L. Wiltshire, J. Cosmol. Astropart. Phys. 06 (2016) 035; A. Krasinski, Phys. Rev. D **94,** 023515 (2016); **97,** 064047 (2018); C. Hellaby and A. Walters, J. Cosmol. Astropart. Phys. 02 (2018) 015; K. Bolejko, J. Cosmol. Astropart. Phys. 06 (2017) 025.

[14] T. Harada and S. Jhingan, Prog. Theor. Exp. Phys. (**2016**) 093E04.

[15] A. Krasinski and K. Bolejko, Phys. Rev. D **85,** 124016 (2012).

[16] R. A. Sussman and K. Bolejko, Classical Quantum Gravity **29,** 065018 (2012).

[17] R. A. Sussman, I. D Gaspar, and J. C. Hidalgo, J. Cosmol. Astropart. Phys. 03 (2016) 012; 06 (2016) 003(E).

[18] R. A. Sussman, J. C. Hidalgo, I. D. Gaspar, and G. Germán, Phys. Rev. D **95,** 064033 (2017).

[19] R. A. Sussman, J. C. Hidalgo, P. K. S. Dunsby, and G. German, Phys. Rev. D **91,** 063512 (2015).

[20] T. Padmanabhan, *Structure Formation in the Universe* (Cambridge University Press, Cambridge, 1993); C. Angrick and M. Bartelmann, Astron. Astrophys. **518,** A38 (2010).

[21] I. Musco, J. C. Miller, and L. Rezzolla, Classical Quantum Gravity **22,** 1405 (2005); I. Musco, J. C. Miller, and A. G. Polnarev, Classical Quantum Gravity **26,** 235001 (2009).

[22] T. Harada, C.-M. Yoo, K. Kohri, K.-i. Nakao, and S. Jhingan, Astrophys. J. **833,** 61 (2016).

[23] M. Bruni, S. Matarrese, and O. Pantano, Astrophys. J. **445,** 958 (1995).

[24] H. van Elst, C. Uggla, W. M. Lesame, G. F. R. Ellis, and R. Maartens, Classical Quantum Gravity **14,** 1151 (1997).

[25] P. Szekeres and A. Lun, J. Aust. Math. Soc. Series B, Appl. Math. **41,** 167 (1999).

[26] B. C. Nolan, Classical Quantum Gravity **20,** 575 (2003).

[27] J. Binney and S. Tremaine, *Galactic Dynamics* (Princeton University Press, Princeton, 2011).

[28] R. A. Sussman, Classical Quantum Gravity **27,** 175001 (2010).

[29] R. A. Sussman, Classical Quantum Gravity **30,** 235001 (2013).

[30] C. Hellaby and A. Krasinski, Phys. Rev. D **66,** 084011 (2002).

[31] P. Szekeres, Phys. Rev. D **12,** 2941 (1975).

[32] A. Coley and D. McNutt, Classical Quantum Gravity **35,** 025013 (2018).

[33] W. Israel, Nuovo Cimento B **44,** 1 (1966).

[34] A. H. Taub, J. Math. Phys. (N.Y.) **21,** 1423 (1980).

[35] W. Bonnor and P. Vickers, Gen. Relativ. Gravit. **13,** 29 (1981).

[36] M. Mars and J. M. M. Senovilla, Classical Quantum Gravity **10,** 1865 (1993).

[37] U. Kirchner, Classical Quantum Gravity **21,** 3845 (2004).

[38] B. Reina, J. M. M. Senovilla, and R. Vera, Classical Quantum Gravity **33**, 105008 (2016).

[39] J. C. Hidalgo, J. De Santiago, G. German, N. Barbosa-Cendejas, and W. Ruiz-Luna, Phys. Rev. D **96**, 063504 (2017).

[40] I. Musco and J. C. Miller, Classical Quantum Gravity **30**, 145009 (2013).

[41] K. Jedamzik, M. Lemoine, and J. Martin, J. Cosmol. Astropart. Phys. 09 (2010) 034.

[42] E. Torres-Lomas, J. C. Hidalgo, K. A. Malik, and L. A. Urea-Lpez, Phys. Rev. D **89**, 083008 (2014).

[43] B. Carr, T. Tenkanen, and V. Vaskonen, Phys. Rev. D **96**, 063507 (2017).